Extended Lee Model for the Turbine Meter & Calibrations with Surrogate Fluids

Jodie G. Pope, John D. Wright, Aaron N. Johnson and Michael R. Moldover

National Institute of Standards and Technology, Gaithersburg, MD, USA

Tel: 301-975-4586, Fax: 301-258-9201, E-mail: jodie.pope@nist.gov, john.wright@nist.gov,

aaron.johnson@nist.gov and michael.moldover@nist.gov

Abstract:

We developed a physical model termed the "extended Lee model" for calibrating turbine meters to account for 1) fluid drag on the rotor, 2) bearing static drag and 3) bearing viscous drag. We tested the extended Lee model using a dual rotor, 2.5 cm diameter turbine meter and accurate flow measurements spanning a 200:1 flow range ($50 < Re < 109{,}000$) with liquid mixtures spanning a 42:1 kinematic viscosity range (1.2×10^{-6} m²/s $< v < 50 \times 10^{-6}$ m²/s). For $Re > 3500$, the model correlates the volumetric flow data within 0.2 %. For $Re < 3500$, deviations from the model increase, reaching 3.6 % at the lowest flows. The same data has a maximum deviation of 17 % from the commonly used Strouhal versus Roshko (or Re) correlation. For all the mixtures tested, the static bearing friction dominates the rotor's behavior when $Re < 1350$ and it results in corrections as large as 51 % of the calibration factor. In a second set of experiments, we compared our calibration using Stoddard solvent (a kerosene-like hydrocarbon with $v \approx 1.2 \times 10^{-6}$ m²/s at 21 °C) with our calibrations using four different mixtures of propylene glycol and water (PG+W). Within the viscosity independent range of this turbine meter ($Re > \sim 7700$), where the Strouhal versus Roshko correlation works well, the PG+W calibrations had an RMS deviation of 0.056 % from the Stoddard solvent calibration; this is well within the long-term reproducibility of the meter. We confirmed this result in the viscosity independent range of a 1.25 cm diameter turbine meter using Stoddard solvent and a 1.2×10^{-6} m²/s v PG+W mixture; these two calibrations agreed within 0.02 %. Therefore, turbine meters can be calibrated with environmentally benign solutions of PG+W and used with more hazardous fluids without an increased uncertainty. The present results also show that using turbine meters at Re below the viscosity independent range of the calibration curve will lead to large errors, unless one accounts for the temperature dependent bearing drag. For example, if the 2.5 cm diameter meter modeled here is calibrated at $Re = 500$ using Stoddard solvent at 20 °C and then used with Stoddard solvent at 30 °C, the decrease of the kinematic viscosity will introduce an error of -0.9 %, unless the temperature dependence of the bearing drag is considered.

Keywords: Turbine meter; calibration; physical model; propylene glycol; kinematic viscosity

Nomenclature

A	cross sectional area of flow [m²]
α	thermal expansion coefficient of meter [°C⁻¹]
$C_D(Re)$	dimensionless fluid drag coefficient that is a function of Reynolds number
$C_D'(Re)$	$C_D(Re)$ with turbine geometric constants included [m⁻³]
C_{D0}'	constant of $C_D'(Re)$ in the laminar rotor boundary layer range [m⁻³]
C_{D1}'	first constant of $C_D'(Re)$ in the transition and turbulent rotor boundary layer range [m⁻³]
C_{D2}'	second constant of $C_D'(Re)$ in the transition and turbulent rotor boundary layer range [m⁻³]
C_{B0}	constant representing the static drag of the ball bearings [kg m²/s²]
C_{B1}	constant representing the viscous drag on the ball bearings [m³]
C_{B2}	constant representing axial thrust and dynamic imbalance drag of the ball bearings [kg m²]
C_{B0}'	constant in term representing the static drag of the ball bearings divided by $\overline{r}^2$ [kg/s²]
C_{B1}'	constant in term representing the viscous drag on the ball bearings divided by $\overline{r}^2$ [m]
C_{B2}'	constant in term representing axial thrust and dynamic imbalance drag of the ball bearings divided by $\overline{r}^2$ [kg]
d	diameter of the meter casing [m]
F	force [N]
f	rotor blade frequency [s⁻¹]
K_f	meter factor based on frequency, f/Q [m⁻³]
K	meter factor based on angular frequency, ω/Q [rad/m³]
K_i	ideal meter factor, ω_i/Q [rad/m³]
k	proportionality constant for static friction forces between the rotor axis and ball bearings [N m²/C²]
l	lead of turbine meter rotor [m]
L	length of the bearing along the axis of rotation [m]
$\dot{m}$	mass flow [kg/s]
m_B	mass of ball bearings [kg]
N	number of rotor blades

Q	volumetric flow [m³/s]
q_1	elemental charge of the rotor axis material [C]
q_2	elemental charge of the ball bearing material [C]
r	radial coordinate vector [m]
$\bar{r}$	root mean square of meter hub and rotor tip radii [m]
R_t	radius of rotor tip [m]
R_h	radius of rotor hub [m]
R_1	inner ball bearing race radius [m]
R_2	outer ball bearing race radius [m]
Re	Reynolds number $= 2R_t u_1 / v$
Ro	Roshko number $= fd^2 / v$
S	surface area of blade [m²]
St	Strouhal number $= K_f \pi d^3 / 4$
t_b	blade thickness [m]
T_d	driving torque [kg m²/s²]
T_r	retarding torque [kg m²/s²]
T_D	torque due to fluid drag on rotor [kg m²/s²]
T_B	ball bearing retarding torque [kg m²/s²]
T_{AT}	torque on bearings due to axial thrust [kg m²/s²]
T_{DI}	torque on bearings due to dynamic imbalance [kg m²/s²]
u_1	velocity of fluid entering the rotor [m/s²]
u_2	velocity of fluid exiting the rotor [m/s²]
Δu	change in magnitude of tangential velocity from the entrance to the exit of the rotor plane [m/s²]
β	angle between rotor axis and rotor blade at corresponding radius [radians]
$\bar{\beta}$	average β corresponding to the root-mean-square radius, $\bar{r}$ [radians]
η	absolute viscosity [N s/m²]
v	kinematic viscosity = absolute viscosity / density [m²/s]
ρ	density [kg/m³]
ω	angular frequency [rad/s]
ω_i	ideal angular frequency [rad/s]

1. Introduction

Turbine flow meters are widely used to measure the flow of valuable fluids such as natural gas and petroleum products. In many cases the meters are calibrated and used with different fluids. The pertinent property that effects turbine meter calibration is kinematic viscosity (absolute viscosity / density, $\nu = \eta/\rho$). Even when a turbine meter is calibrated and used with a single fluid, the kinematic viscosity might change between the time of calibration and the time used because of the temperature-dependence of this quantity. Because there is poor understanding of how the kinematic viscosity affects turbine meter calibrations, expensive, extra calibrations occur. For instance, in petroleum custody transfer (billing) applications, a turbine meter is field re-calibrated each time the product in the pipeline changes [1]. In other applications, a single turbine meter is used to measure flows of fluids with very different kinematic viscosities such as jet fuel (1.2×10^{-6} m^2/s) and hydraulic oils (16×10^{-6} m^2/s to 100×10^{-6} m^2/s). To ensure accurate flow measurements over such a wide range of kinematic viscosities and to calibrate meters under conditions that match the meter application, calibration laboratories use three approaches 1) changing the fluids in their calibration standards, 2) maintaining multiple calibration standards with different fluids in each one, or 3) varying the temperature of the calibration fluid (thereby raising the uncertainty of the measurement).

The first goal of this paper is to present an experimentally validated physical model that explains the influence of kinematic viscosity on turbine meter performance. The second goal of this paper is to demonstrate, both from experiment and from the logic of the model, that mixtures of propylene glycol and water (PG+W) are an acceptable surrogate fluid for hydrocarbon liquid flow calibrations.

Most laboratories that calibrate turbine meters for jet fuel applications use a surrogate fluid called Stoddard solvent (MIL-PRF-7024E Type II, a light mineral oil, $\nu \approx 1.2$ x 10^{-6} m^2/s at 20 °C) that is less flammable and toxic than jet fuel. Recently, Arnold Air Force Base calibration laboratories and NIST began using PG+W mixtures instead [2] since they are biologically and environmentally benign whereas there is evidence to the contrary for Stoddard solvent [3]. A 1 % molar mixture of PG+W matches the kinematic viscosity of jet fuel and pure PG has a kinematic viscosity of approximately 50×10^{-6} m^2/s, which is in the middle of the range of hydraulic oils at 21 °C. Calibration laboratories are interested in utilizing PG+W mixtures to 1) decrease the cost of maintaining multiple standards with fluids of various kinematic viscosities, 2) reduce pollution and provide a biologically benign environment for workers, 3) reduce the danger associated with maintaining multiple standards that require the involvement of the fire department during the use of flammable fuels, and 4) decrease the expense and risk of disposal of the harmful substances [2, 4]. Furthermore, PG+W mixtures have

the benefit of a lower volumetric thermal expansion coefficient and a lower heat capacity than Stoddard solvent resulting in lower storage effect errors and better uncertainty [5].

Physical models for the turbine meter based on the momentum and airfoil approaches were publish by Lee and his colleagues [6, 7] and Rubin *et al*. [8] in the 1960s. Their work and others', which are included in Baker's turbine meter review article [9] are reviewed here in our derivation of the physical model. We call the model presented here the "extended Lee model" because our fundamental expression based on the momentum approach (Equation 11) was derived by Lee and Karlby [7] and because the important torques on the rotor (as presented in Equation 18) were described by Lee and Evans [6]. Lee and his colleagues have set the foundation for our work by identifying the drag terms via the momentum approach. However, in their use of the model, they simplified the effects of bearing drag terms because gas was the working fluid making viscosity changes insignificant [6] or because they considered such torques as constant over the range of Reynolds (*Re*) values of interest [7]. By neglecting these terms they did not explain why multiple viscosity calibration curves separate or "fan" at low *Re* numbers (see Figure 1(a)). They focused on the upper end of the meter range, where the meter factor ($K_f = f/Q$) is an approximately linear function of the *Re* number or the Roshko number (*Ro*). In this region, the calibration data for various kinematic viscosities collapses onto a single calibration curve (see Figure 1(a) and Appendix B). More recently Tsukomoto and Hutton [10] presented an analytical model based on airfoil theory and compared it to experimental data for four liquids with different viscosities. They explained the transition from turbulent to laminar flow in the rotor blade boundary layer generates the characteristic "hump" in the curve (see Figure 1(a)). However, their model lacks the term that is the strongest contributor to the fanning phenomenon, the bearing static drag term (see section 4.1 and Figure 5). Surface fits using a third dimensionless term have shown success for predicting meter performance over a wide range of viscosities and flows, however, they lend no insight as to why the multiple viscosity curves fan at low *Re* numbers [11]. In general, prior researchers have focused on the relationship between meter performance and geometry to optimize meter design. Instead of improving turbine meter design, this work aims to look at the entire *Re* range over which the turbine meter's rotors will physically turn to provide a sound reason for why deviations in viscosity of a liquid cause fanning in a meter's calibration curve at *Re* numbers approaching zero. We extend on Lee's work to explain this phenomenon and validate the model experimentally at low flows where bearing drag terms are significant.

In this paper, a model based on physical phenomena for the turbine meter is validated utilizing data over a flow range of 200:1 (0.57 L/min to 151 L/min) and PG+W mixtures with kinematic viscosity ranging from 1.2×10^{-6} m^2/s to 50×10^{-6} m^2/s. This wide range of flows and kinematic viscosities exposes several

phenomena shown in Figure 1(a) that are well explained by the extended Lee model: 1) there is a peak in the meter factor at $Re \approx 4450$, 2) meter factor versus Re plots work well in what we call the "viscosity independent range" of the turbine meter, in this case for $Re > 7700$, 3) at $Re < 7700$, a fanning or non-convergence of the curves occurs, most pronounced for $v < 5 \times 10^{-6}$ m^2/s, and 4) at $Re < 7700$ and for $v > 5 \times 10^{-6}$ m^2/s, the calibration curves coincide to a high degree again. We have named the range of the calibration curve where fanning occurs the "bearing dependent range" because, as will be demonstrated, the bearings are responsible for the fanning phenomenon. The solid lines in Figure 1(a) are the meter factors calculated from the extended Lee model when coefficients related to fluid drag on the rotor and bearing drag are fitted to the experimental data. At all but the lowest flows and at kinematic viscosities of 1.2×10^{-6} m^2/s, 1.5×10^{-6} m^2/s, and 1.9×10^{-6} m^2/s, the agreement between the model and experiment is better than 2 % (Figure 1(b) & 1(c)). This agreement is excellent considering that the model corrections are as large as 61 % of the ideal meter factor (K_i), the theoretical meter factor if no retarding torques on the rotor exist.

We also demonstrate from experiment that when using turbine meters within the viscosity independent range of the calibration curve (*i.e.* at Re values above the K factor peak) PG+W mixtures give the same calibration results as Stoddard solvent within the uncertainty of the tests (see Section 4.4).
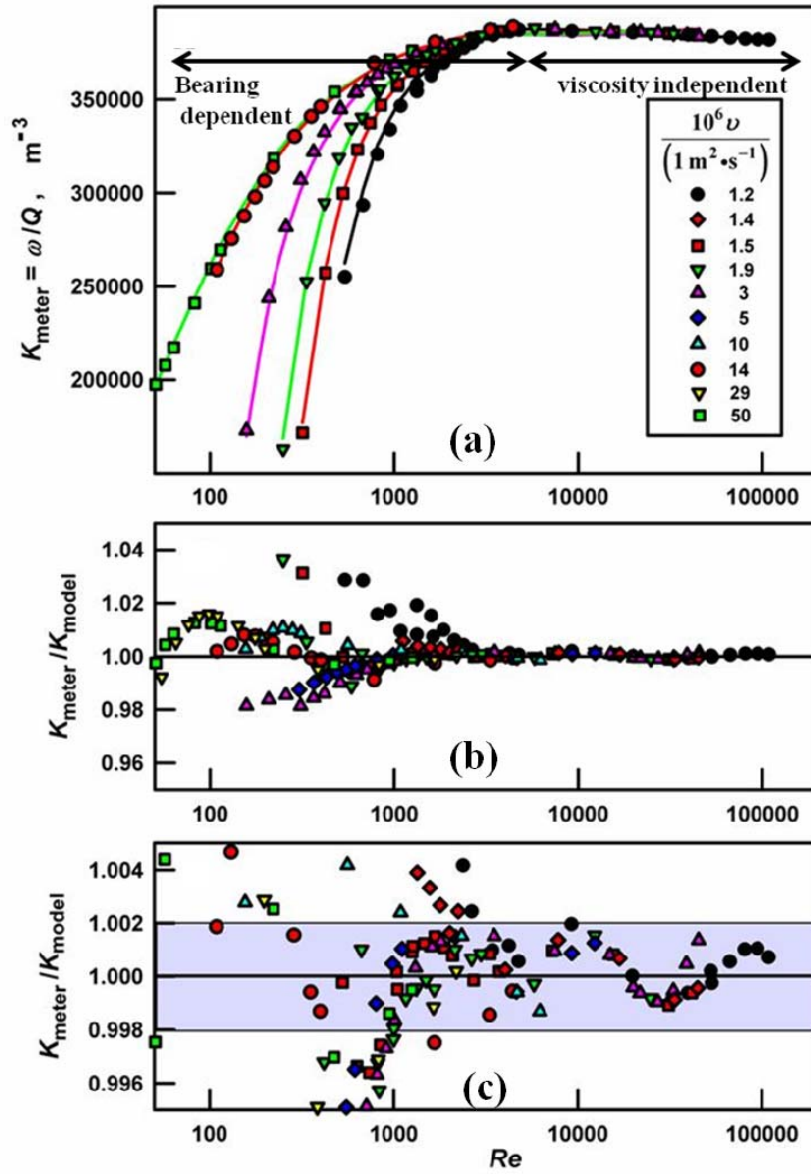
Figure 1: (a) Calibration curve of the upstream rotor of a dual rotor turbine meter with various kinematic viscosity solutions of PG+W. Some tested kinematic viscosities are omitted from (a) for clarity but are shown in (b) and (c). In the bearing dependent range, (Re < 7700) the different curves fan out at viscosities < 5×10^{-6} m^2/s and then they converge again at higher viscosities. The lines are a fit to the experimental data (symbols) using the fitted Lee model. Re = Reynolds number of the pipe. (b) and (c) Ratio of computed to experimental values of K. In (c), the shaded band spanning ± 0.2 % represents the fluid property and long term calibration uncertainties.

2. Materials and Methods

United States Pharmacopeia grade (i.e. safe for human consumption) propylene glycol was mixed with reverse osmosis water to generate mixtures ranging in kinematic viscosity from 1.2×10^{-6} m^2/s to 50×10^{-6} m^2/s at 21 °C. The NIST 20 liter hydrocarbon liquid flow standard was used to generate calibration curves for a turbine

meter at temperatures between 20 °C and 22 °C [5]. The system was pressurized to approximately 20 psi, more than double the pressure drop across the meter for the majority of PG+W mixtures tested (to avoid cavitation). The NIST standard is a piston prover in which the piston displaces a known volume of fluid during a measured time interval. The prover has a 95 % confidence level uncertainty of 0.073 % (All uncertainties herein are approximately 95 % or $k = 2$ values unless otherwise stated). Data was collected from a 2.5 cm and a 1.25 cm diameter, dual rotor, turbine meter (Figure 2). Meters of this size and design are often used to measure the flow of jet fuel and hydraulic oil. The 2.5 cm meter was used to evaluate the extended Lee model and both meters were used to compare calibration curves generated using PG+W mixtures and Stoddard solvent. We initially used the data from the upstream rotor alone to evaluate the extended Lee model since we anticipated flow disturbances upstream from the second rotor would be a complicating factor. However, the model was tested on the downstream and summed rotor data too (see Section 4.2). Data were collected starting at the minimum flow that would overcome bearing static friction and initiate rotation of the turbine meter rotor (for some of the PG+W mixtures) and to the low end of the turbulent flow regime (65 % of manufacturer recommended maximum). We used such low flows to emphasize the phenomena that limit the viscosity independent range where the meter is usually used. This allowed us to test the functional forms of the static and dynamic bearing drag. The upper flow limit (151 L/s) was set by the specifications of the NIST 20 liter piston prover.
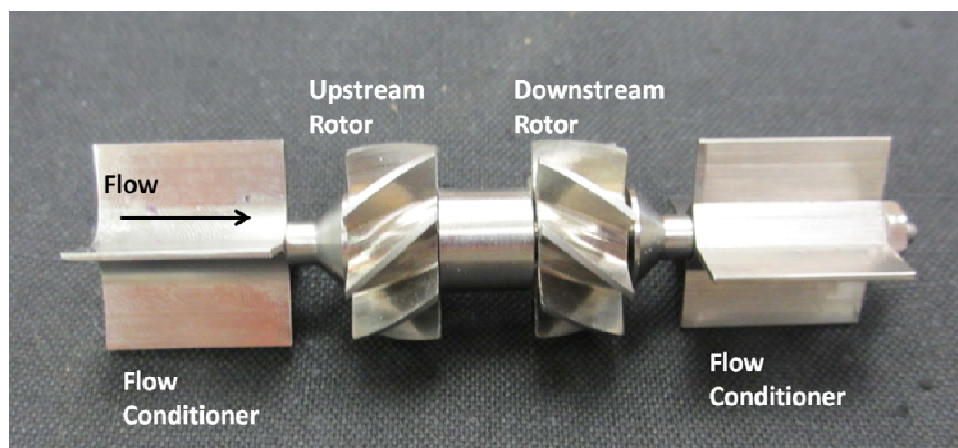

Figure 2: The internal assembly of the 2.5 cm dual rotor turbine meter studied in this manuscript. Omitted with casing is the two radio frequency pickoffs that measure the frequency at which each rotor is spinning.

For each mixture, 5 data points were taken at each flow. The system was then shut down and restarted and the experiment repeated to assure meter reproducibility that ranged from 0.093 % at the highest flow to 0.18 % at the lowest flow. (These are the worst case values, most reproducibilities were an order of magnitude lower.)

8

A Rudolph Research Analytical densimeter, model DDM2911, with manufacturer stated uncertainty of 0.005 % was used to determine density and an Anton Paar viscometer, model AMVn, with uncertainty stated by the manufacturer of 0.5 % was used to determine the kinematic viscosity of each mixture.[A] The resultant density and kinematic viscosity data agree with other reports of PG+W properties within 1 % [12, 13]. The accuracy to which the kinematic viscosity needs to be known for calibration depends upon the Re range over which the meter will be used. As will be demonstrated in this paper, it does not need to be known accurately for flow measurements in the viscosity independent range of the turbine meter. However, to maintain the lowest possible uncertainty associated with using the meter in the bearing dependent range, a model that accounts for bearing drag and accurate kinematic viscosity values is necessary. The partial derivative of the extended Lee model with respect to kinematic viscosity was determined and normalized by multiplying by v/K to demonstrate the accuracy to which the kinematic viscosity must be known in the bearing dependent range. It was found that $\left(v/K\right)\left(\partial K/\partial v\right) \approx -27\left(Re\right)^{-0.9}$ reaches -1 near $Re = 50$ for the 2.5 cm turbine. Thus, a 1 % error in kinematic viscosity will introduce a 1 % error in the measured flow near $Re = 50$.

3. Lee Model for the Turbine Flow Meter

The relationship between the fluid flow through a turbine meter and its rate of rotation is dependent on many parameters that are impractical to measure with low uncertainty, *e.g.* blade angles, tip clearance and bearing friction. Hence our goal is not to derive a physical model that attempts to relate precisely measured meter geometry to the meter calibration. Instead we seek the functional form of the physical model that we can fit to flow calibration data. The model coefficients determined from a limited number of test flows and kinematic viscosities during calibration can then be used to interpolate data for other conditions.

There are two approaches described in the literature to account for the characteristics of the calibration curve for turbine flowmeters. The first approach describes fluid driving torques in terms of aerodynamic lift and drag via airfoil theory, while the second describes it in terms of momentum exchange [14]. In this work, we have chosen the momentum approach because it leads to the functional form of the calibration curve without knowledge of the meter's internal geometry.

The K factor of a turbine meter is the ratio of angular frequency to the volumetric flow

---

[A] Certain commercial equipment is identified in this paper to foster understanding. Such identification does not imply recommendation or endorsement by NIST, nor does it imply that the equipment identified is necessarily the best available for the purpose.

$$K = \frac{\omega}{Q}. \tag{1}$$

It is usually determined by calibration of the meter against a flow reference. The ideal K factor (K_i) can be calculated from the geometry and dimensions of the turbine meter by considering the volume of fluid passing for a single revolution of the rotor. For a rotor that has no retarding torque, the fluid will displace the rotor without any deflection of the fluid velocity vector (zero tangential velocity, see Figure 3(b)). In this case, the volume of liquid passing through the rotor for one revolution is equal to the cross sectional area of flow multiplied by the lead (l) where the lead is the distance in the axial direction the rotor would traverse in one revolution if it acted like a screw thread on the fluid [8].

Calling the angle between the rotor axis and the blade β, by geometry one can write:

$$\tan\beta = \frac{\text{perimeter swept per revolution}}{\text{linear advance per revolution}} = \frac{2\pi r}{l}, \tag{2}$$

which can be rearranged to give the following expression for the lead:

$$l = \frac{2\pi r}{\tan\beta} \tag{3}$$

Note that for a helical blade, the lead is the same for all radial displacements along the blade and β is a function of the radial displacement from the axis, *i.e.* Equation 3 remains valid for the helical blade as long as consistent pairs of β and r values are used.

Then K_i can be calculated by taking the ratio of the angle swept to the volume passed by the rotor:

$$K_i = \frac{\omega_i}{Q} = \frac{\text{angle swept per revolution}}{\text{volume swept per revolution}} = \frac{2\pi}{lA} = \frac{\tan\overline{\beta}}{\overline{r}A}, \tag{4}$$

where ω_i is the ideal angular frequency. The quantity A represents the cross sectional area of flow between the rotor hub and tips, $A = \pi(R_t^2 - R_h^2) - (R_t - R_h)t_b N$, where t_b is the thickness of the rotor blade and N is the number of blades. The quantity $\overline{r}$ is the root-mean-square of the hub and tip radii, $\overline{r}^2 = (R_t^2 + R_h^2)/2$ and $\overline{\beta}$ is the

blade angle corresponding to $\bar{r}$. Equation 4 shows that for the ideal case, the meter calibration factor is a constant that is determined solely by the meter geometry and dimensions, *i.e.* it is independent of the flow.
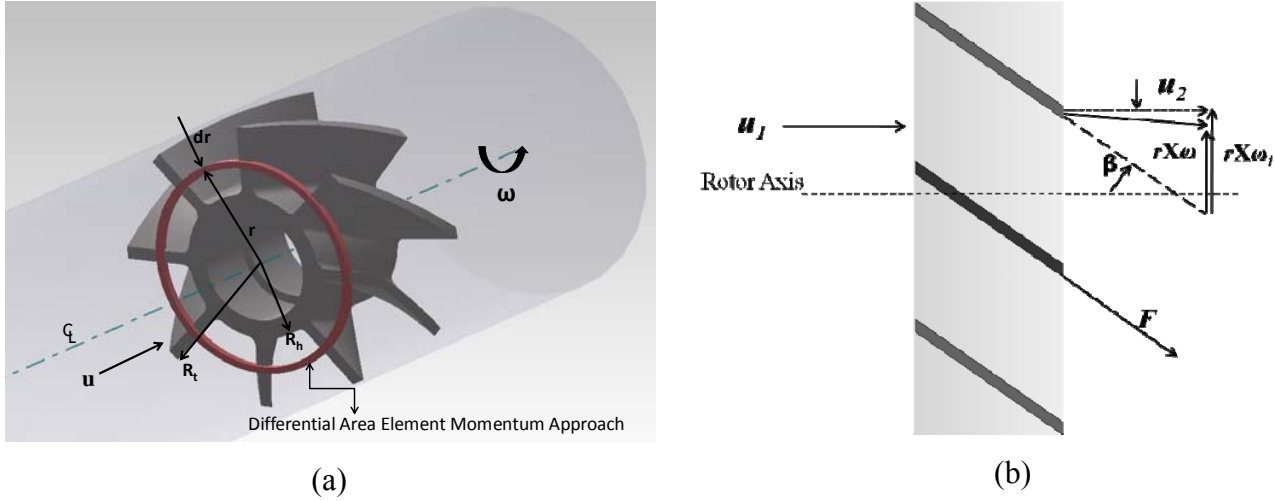

Figure 3: (a) Diagram of turbine meter rotor showing differential area element. (b) Vector diagram for an axial turbine flowmeter. The difference between the ideal (subscript i) and the actual tangential velocity is a consequence of the rotor retarding torques. (Part (b) of this figure was re-created from Wadlow's review [14]).

In the case of a real rotor, retarding torques due to fluid drag on the blades and drag in the rotor bearings cause what is often called a "slip velocity" resulting in a lower rotor angular velocity than the ideal case. The fluid passing through the rotor is deflected by the blade and there is a non-zero tangential velocity at the rotor outlet (see Figure 3(b)). This change in momentum of the fluid crossing the rotor inlet and outlet planes is the driving force opposing the retarding torques. In the momentum approach to the turbine meter physical model, the real, steady-state angular frequency of the rotor satisfies the condition of equilibrium of the driving and retarding torques on the rotor, *i.e.* $T_d = T_r$. Applying conservation of momentum to the control volume containing the rotor and neglecting pressure effects leads to:

$$\vec{F} = \dot{m}\left(\vec{u}_1 - \vec{u}_2\right), \tag{5}$$

where $\dot{m}$ is the mass flow through the meter and $\bar{u}$ is the fluid velocity vector. For the annular differential area element shown in Figure 3(a), this expression becomes:

11

$$dF = \frac{\rho Q}{A}(2\pi r dr)\Delta u, \qquad (6)$$

where ρ is the fluid density, $\Delta u = \|u_1 - u_2\|$ represents the change in the tangential velocity of the fluid between the entrance and the exit planes of the rotor, r is the radial coordinate, and $\rho Q/A$ represents the unit area mass flux. The torque imposed on the differential area element by the change in fluid momentum is:

$$dT_r = rdF = r\frac{\rho Q}{A}(2\pi r dr)\Delta u. \qquad (7)$$

The velocity vector diagram in Figure 3(b) shows that the change in tangential fluid velocity is related to the difference in the ideal and actual angular velocity of the rotor (This analysis assumes that the rotor has sufficient solidity that all of the fluid passing through the rotor exits with the same tangential velocity)

$$\Delta u = r\omega_i - r\omega. \qquad (8)$$

Considering the annular differential area element and integrating the torque over the cross sectional area of the rotor gives:

$$T_r = \int_{R_h}^{R_t} r\left(\frac{\rho Q}{A}\right)(2\pi r)r(\omega_i - \omega)dr. \qquad (9)$$

Neglecting the cross-sectional area the rotor blades occupy, the solution to Equation 9 is:

$$T_r = \frac{\rho Q}{2}\left(R_t^2 + R_h^2\right)(\omega_i - \omega). \qquad (10)$$

Using the root-mean-square radius previously defined, rearranging and using Equation 4 gives:

$$K = \frac{\omega}{Q} = \frac{\tan\bar\beta}{\bar r A} - \frac{T_r}{\bar r^2 \rho Q^2}. \qquad (11)$$

12

Equation 11 is the fundamental expression of the turbine meter Lee model based on the momentum approach: the ideal K factor (first term on the right hand side) is reduced due to the retarding torques (second term) to obtain the real K factor. In the following paragraphs, we extend the Lee model further by including expressions for the retarding torques related to fluid drag and bearing friction drag.

From Wadlow's review on turbine meter theory [14], the torque exerted on the rotor system due to fluid drag on the blades is:

$$T_D = \frac{\rho Q^2 NS \sin \beta}{2\pi^2 \bar{r}^3} C_D(Re),$$
(12)

where S is the blade surface area. This term is multiplied by a dimensionless drag coefficient that is a function of Re, $C_D(Re)$, and can be rearranged to be in the form presented in Equation 11:

$$\frac{T_D}{\bar{r}^2 \rho Q^2} = \frac{NS \sin \beta}{2\pi^2 \bar{r}^5} C_D(Re) = C_D'(Re).$$
(13)

The dimensionless drag coefficient C_D can be combined with the meter specific geometric parameters $(NS \sin \beta / 2\pi^2 \bar{r}^5)$ to give C_D' with units of m^{-3} as shown in Equation 13. The fluid drag coefficient depends on whether the boundary layer on the rotor blade surface is laminar or turbulent. In the laminar Re range, $C_D'(Re) = C_{D0} / Re^{0.5}$ and in the transition - turbulent range we found the best form to fit the experimental data is $C_D'(Re) = C_{D1} + C_{D2} / \log_{10} Re$. Therefore the fluid drag term is:

$$\frac{T_D}{\bar{r}^2 \rho Q^2} = \frac{C_{D0}'}{Re^{0.5}}, \text{ for } Re < 4450 \text{ and}$$
(14)

$$\frac{T_D}{\bar{r}^2 \rho Q^2} = C_{D1}' + \frac{C_{D2}'}{\log_{10} Re}, \text{ for } Re > 4450.$$
(15)

There are three components involved in the torque due to bearing drag, T_B [6]: 1) that which is independent of rotor speed that can be thought of as Coulomb type friction or static drag (C_{B0}), 2) that which increases almost linearly with rotor speed and is mainly due to viscous drag in the bearing ($C_{B1} \rho v \omega$) and 3) that which increases with the square of the rotor speed, mainly due to axial thrust and dynamic imbalance of the rotor system ($C_{B2} \omega^2$). The parameters C_{B0}, C_{B1} and C_{B2} are meter specific constants that are derived in Appendix A. They have the dimensions of kg m^2/s^2, m^3 and kg m^2 respectively. The bearing drag torque can be written as:

$$T_B = C_{B0} + C_{B1}\rho v \omega + C_{B2}\omega^2. \tag{16}$$

Equation 16 is rearranged in the form of the retarding torque in Equation 11, to obtain:

$$\frac{T_B}{\overline{r}^2 \rho Q^2} = \frac{C'_{B0}}{\rho Q^2} + \frac{C'_{B1}v\omega}{Q^2} + \frac{C'_{B2}\omega^2}{\rho Q^2}, \tag{17}$$

For a detailed derivation of these terms as they appear in Equation 17 see Appendix A.

Equations 14 (or 15) and 17 can now be inserted into Equation 11 to yield the model equation:

$$\frac{\omega}{Q} = K_i - C'_D(Re) - \frac{C'_{B0}}{\rho Q^2} - \frac{C'_{B1}v\omega}{Q^2} - \frac{C'_{B2}\omega^2}{\rho Q^2}, \tag{18}$$

where the fluid drag term is written as $C'_D(Re)$ for convenience to represent both Equations 14 and 15. Equation 18 can be rearranged as a quadratic function of Q, and solving it yields the working equation:

$$Q = \frac{1 + \sqrt{1 + 4\left(\frac{K_i}{\omega} - \frac{C'_D(Re)}{\omega}\right)\left(\frac{C'_{B0}}{\rho\omega} + C'_{B1}v + \frac{C'_{B2}\omega}{\rho}\right)}}{2\left(\frac{K_i}{\omega} - \frac{C'_D(Re)}{\omega}\right)}. \tag{19}$$

For practical purposes, the coefficients in Equation 18 can be determined from a calibration of a turbine flowmeter in multiple kinematic viscosity liquids. Instead of using Reynolds number for the fluid drag term, it

14

can be put in terms of the Roshko number with the advantage that no iteration would be required to use Equation 19 since *Re* contains the volumetric flow and *Ro* does not. Therefore, the user would only need to know the frequency of the meter and the kinematic viscosity and density of the fluid to use Equation 19. As will be shown in the following sections, bearing correction terms are not necessary if the meter is used in the viscosity independent range of the calibration curve and *K* vs. *Re* or *St* vs. *Ro* curves work well despite changes in the kinematic viscosity of the fluid being metered. The extended Lee model is useful and will lower the uncertainty in the measurement if the meter is to be used in the bearing dependent range. However, such a calibration would be a painstaking one and it is advised to use the meter in the viscosity independent range for low uncertainty measurements.

4. Results and Discussion

4.1. The Extended Lee Model Explains the Experimental Data

Figures 1(b) and (c) show the ratio of the *K* factor calculated from our model and the actual *K* factor for all PG+W mixtures tested for the upstream rotor of a dual rotor turbine meter. The standard deviation of the residuals from the ideal value of unity is 0.77 %. The model correlates the meter *K* factor within 0.2 % for *Re* > 3500. At *Re* < 3500, deviations from the model increase to 3.6%. The good agreement between the fitted model and the measurements gives us confidence that the extended Lee model contains the significant phenomena, at least for this particular turbine meter design.

Due to the shape of the multiple viscosity calibration curves, fitting the model to the data was done by trial and error where the standard deviation in the residuals and the minimum and maximum of these residuals was observed while changing the model coefficients one at a time. A general approach for fitting Equation 19 to multiple viscosity curves of a meter is as follows. Because the ideal *K* factor is a constant from which the retarding torques are subtracted, it was determined first. This value can be estimated by where the calibration curves are approximately linear and keeping in mind it must be greater than all *K* values. Next the fluid drag coefficient for the laminar range was determined as the fluid drag term shifts the slope of the calibration curves in a uniform manner. An initial value for this drag coefficient will create a slope that mimics the experimental data in the laminar range of the calibration curves. The bearing viscous drag coefficient was then determined as it further adjusts the slope of the calibration curves in a uniform manner and introduces slight fanning, but only in the bearing dependent range. This term can be estimated by observing how the model fans and observing when the fanning appears to mimic the experimental data. The bearing static drag coefficient was fitted next as it further increases the fanning of the curves in the bearing dependent range. Once all the coefficients were determined and optimized by reducing the residuals, the fluid drag coefficients for the turbulent range were

determined as it had to be continuous with the function in the laminar range. Lastly a solver was used to determine if the bearing drag coefficient due to axial thrust and dynamic imbalance could improve the fit, and it was found to be insignificant ($< 0.2\%$ of K_i for all Re values). Once reasonable estimates of the coefficients were known by the trial and error approach, a solver that uses a least squares fit algorithm was used to optimize each coefficient over the entire data range.

The fitted extended Lee model allows us to understand the complex behavior of the turbine meter in various flow ranges, such as the fanning observed in the bearing dependent range. The individual terms of Equation 18 are plotted in Figures 4 to 6 versus Re in the left panel and versus volumetric flow Q in the right panel. These figures display the advantages of using Re instead of Q for the horizontal axis in calibration curves (see also Appendix B). We note that the model coefficients used to generate these figures apply only to this particular meter, but a meter with a different design is likely to have qualitatively similar behavior to that shown here.
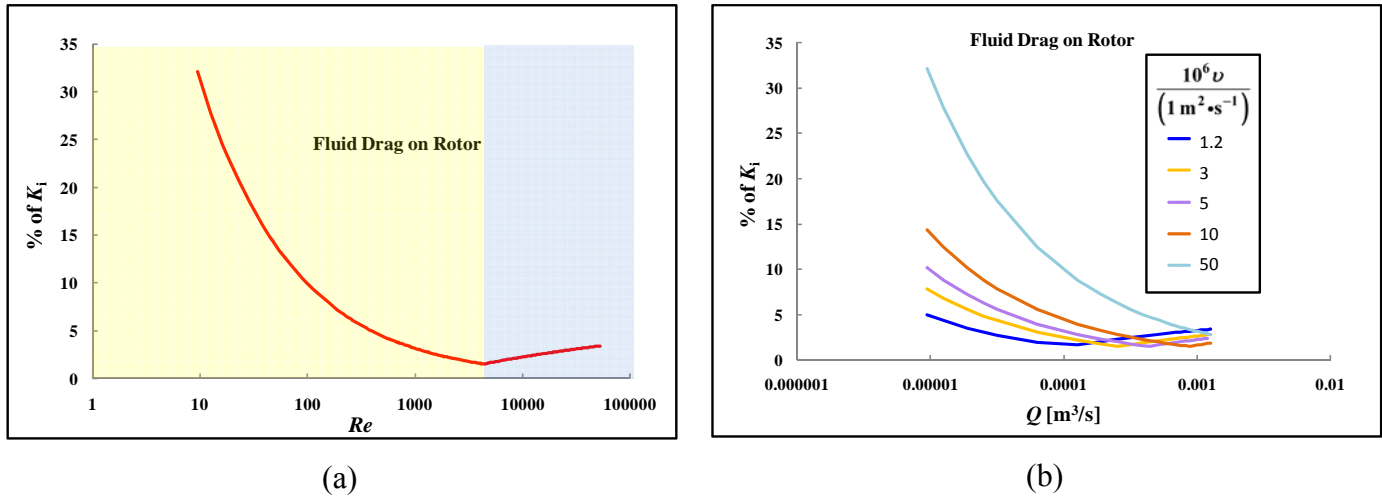

(a)   (b)

Figure 4: (a) The fluid drag term uses two functions of Re for the laminar (yellow) and transition - turbulent (blue) ranges. When plotted versus flow (b), data does not collapse.

Figure 4 presents the fluid drag term, $C_D'(Re)$, of the extended Lee model as a percent of K_i versus Re (a) and volumetric flow (b). The change in the Re dependence at $Re = 4450$ is clear as the laminar boundary layer on the rotor begins transition to turbulent flow and the two regions are highlighted with color in the figure. At $Re = 4450$, the fluid drag correction is at its minimum (1.6 %), causing the peak in the calibration curve (Figure 1(a)) where the turbine is closest to the ideal behavior. At higher Re numbers, the fluid drag correction increases as a weak function of Re. As shown in Figure 7, the fluid drag term dominates at the higher Re numbers and its dominance and Re dependence leads to the viscosity independent range of turbine meter

performance shown in Figure 1(a). Since the fluid drag correction is a function of *Re*, it does not disrupt the collapsing of calibration data onto a single calibration curve when one follows the commonly used *K* vs. *Re* (or Strouhal vs. Roshko plots, see Appendix B).
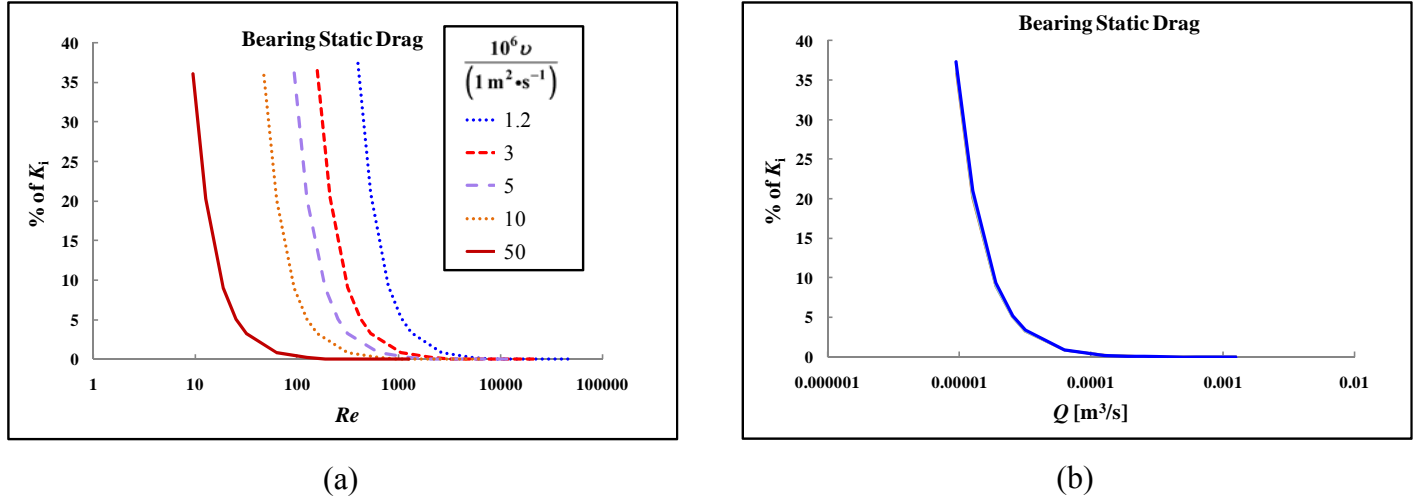

(a)

(b)

Figure 5: (a) The bearing static drag term is the main reason for the fanning of the calibration curve as can be seen when plotted against Re. (b) However, when plotted against flow, this term's curves fully collapse.

Figure 5 plots the bearing static drag term, $C'_{B0}/(\rho Q^2)$, of the extended Lee model as a percent of K_i versus *Re* (a) and volumetric flow (b). This term is primarily responsible for the fanning observed in the calibration curve at lower flows shown in Figure 1(a). Its proportionality to $1/Q^2$ leads to several, separate curves dependent on the kinematic viscosity when plotted vs. *Re*. The fanning observed in the normal presentation of turbine meter data (*K* vs. *Re* or *St* vs. *Ro* plots) is primarily a consequence of this term's dependence on flow, not *Re*.
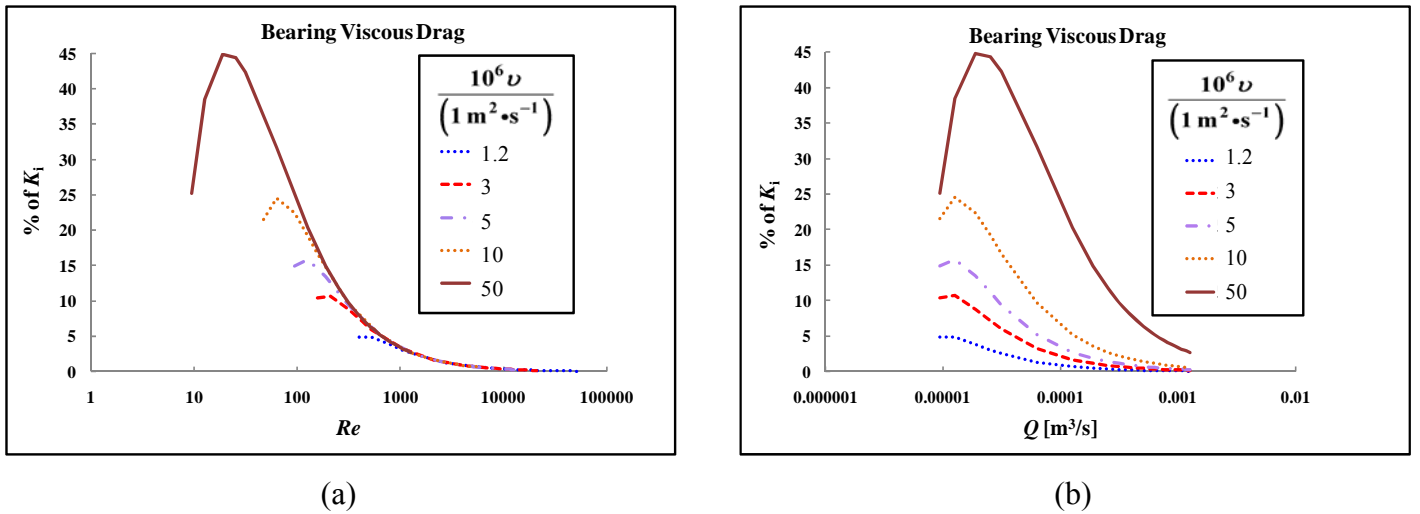

(a)

(b)

Figure 6: (a) The bearing viscous drag is slightly responsible for the fanning phenomenon as can be seen when plotted against Re.

Figure 6 shows the bearing viscous drag term, $C_{B1}' \omega v/Q^2$, of the extended Lee model as a percentage of K_i versus Re (a) and versus volumetric flow (b). This correction has a hybrid behavior: At higher Re values, it is well collapsed by Re, but the collapsing fails at lower values. An explanation for this is, at higher flows where the turbine operates near the ideal model, ω is proportional to Q and the bearing viscous drag term can be approximated by $C_{B1}' v/Q$, a term that is proportional to $1/Re$ and hence collapses to a single curve when plotted vs. Re for various kinematic viscosity values. However, at low flows, the corrections to the ideal model become significant as ω is no longer proportional to Q, leading to a separation of the various kinematic viscosity curves. Hence, the bearing viscous drag term is partially responsible for fanning of the calibration curves shown in Figure 1(a).

The coefficient for bearing drag due to axial thrust and dynamic imbalance C_{B2}' was negligible for this turbine meter (< 0.19 % of K_i), as would be expected for a well functioning turbine meter. Since this term increases with the squared angular frequency of the rotor, it does not collapse with Re. If it were significant, the calibration curve would not converge in the viscosity independent range for fluids with different kinematic viscosities.

In Figure 7, we plot the three significant correction terms for three kinematic viscosity cases to compare the relative importance of the various corrections under different conditions. Each of the corrections is dominant under different Re or v conditions, leading to the complex calibration curve shown in Figure 1(a).
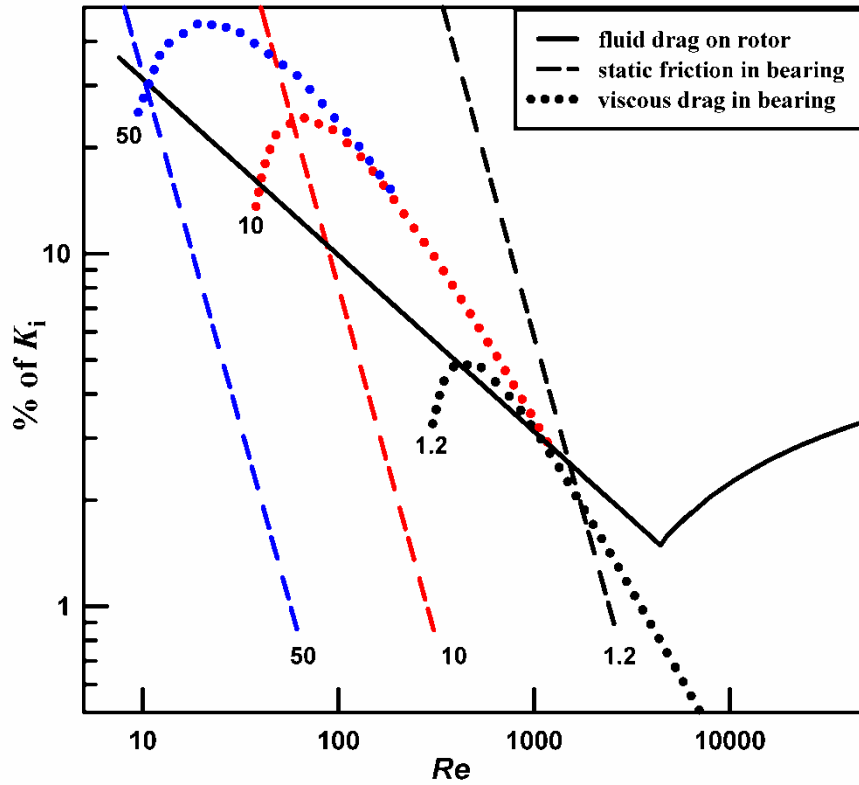
Figure 7: The significant correction terms for various kinematic viscosity solutions. The kinematic viscosities shown have the units of 10^{-6} m^2/s.

At the lowest kinematic viscosity presented in Figure 7, 1.2×10^{-6} m^2/s, the bearing static drag term dominates the other two mostly *Re*-dependent corrections at low *Re* values. Since this term is flow dependent, not *Re* dependent (see Figure 5), its dominance causes strong fanning of the *K* vs. *Re* plot as seen in Figure 1(a). The fanning phenomenon diminishes for the higher kinematic viscosities because at even lower *Re* values, the fluid drag and bearing viscous drag corrections together overwhelm the bearing static drag term. However, as explained before and shown in Figure 6, the bearing viscous drag term is not perfectly collapsed by *Re* and in fact some fanning is still visible in Figure 1(a) for the highest kinematic viscosity measurements at the lowest *Re* values.

It should be noted that the transition *Re* number between a laminar or turbulent boundary layer for the fluid drag term and the *Re* at which fanning occurs (the upper limit of the bearing dependent range) are not coincident. For the upstream rotor of this meter the values are 4450 and 7700 (for 0.1 % fanning) respectively. The peak *K* value is dependent on the boundary layer transition and does not identify the minimum operating *Re* to avoid bearing dependent uncertainties. To identify the bearing dependent range, the turbine should be calibrated in liquids of various kinematic viscosities.

4.2. Extension of the Model to Downstream and Dual Rotor Measurements

As previously mentioned, we used the data from the upstream rotor (Figure 1) of a dual rotor meter (Figure 2) to validate the extended Lee model because we expect disturbances of the entering velocity profile generated by the upstream rotor to disrupt application of the model to the downstream rotor. However, the model was tested on the downstream and summed rotor data as shown in Figure 8. The data set was limited compared to the data set for the upstream rotor due to software limitations for automatic data collection by the 20-L prover. The same kinematic viscosities were used; however, the flow range was reduced to 1.9 L/min to 76 L/min, compared to 0.57 L/min to 151 L/min for the upstream rotor and the reduced flow range leads to less fanning in Figure 8 than in Figure 1.

The data could be fitted using the extended Lee model. However, the function of Re that the fluid drag term depends upon had to be altered from that of Equation 14 to obtain good results for the bearing dependent range for the downstream rotor. For the viscosity independent range the function of Re the downstream rotor takes is the same form as for the upstream rotor (Equation 15) but the transition is at $Re = 2500$, determined by where the peak in the meter factor curve occurs. The altered function for the downstream rotor for $Re < 2500$ is:

$$C_D'(Re)_{\text{down}} \left[\text{m}^{-3} \right] = 698200 + 216800 \log Re - 616460 \log Re^2 + 242100 \log Re^3 - 28330 \log Re^4 \quad (20)$$

The alteration in the functional form of the fluid drag correction term improved the goodness of fit for the downstream rotor in the bearing dependent range to 1.5 % from 3 %.; However it had no significant effect on the goodness of fit for the upstream rotor.

For the downstream rotor, the fitted model predicts the volumetric flow within 0.64% for $Re > 2500$ and within 1.5 % for $Re < 2500$. The second rotor reaches a maximum K factor at $Re = 2500$ vs. 4450 for the upstream rotor, perhaps because flow disturbances by the upstream rotor cause laminar to turbulent boundary layer transition at a lower Re. The standard deviation of the residuals from the ideal value of unity is 0.33 %.

For the summed rotors, the individual terms of Equation 18 were added:

$$\frac{\left(\omega_{\text{up}} + \omega_{\text{down}} \right)}{Q} = \left(K_{i,\text{up}} + K_{i,\text{down}} \right) - \left(C_D'(Re)_{\text{up}} + C_D'(Re)_{\text{down}} \right) - \frac{\left(C_{B0,\text{up}}' + C_{B0,\text{down}}' \right)}{\rho Q^2} - \left(\frac{C_{B1,\text{up}}' v \omega_{\text{up}} + C_{B1,\text{down}}' v \omega_{\text{down}}}{Q^2} \right), \quad (21)$$

where the bearing drag due to dynamic imbalance and axial thrust has been excluded as it was found to be negligible. Equation 21 has unique features compared to the single rotor case; it accounts for differences in the bearing viscous drag term and the different transition Re values for each rotor and thus fits the summed rotor data better than Equation 18. For the summed rotors, the model predicts the volumetric flow within 0.24 % for $Re > 1555$ and within 1.1 % for $Re < 1555$. The summed rotor calibration curve has a maximum K factor at $Re = 3320$. The standard deviation of the residuals from the ideal value of unity is 0.35 %.

The coefficients that optimize the fit of the model to the experimental data and the transition Re value for the fluid drag term are listed in Table 1. Figure 8 compares the measured data and the model for each rotor and the sum using the limited flow data.

Table 1: Values for the fitted coefficients in the physical model. The angle β that corresponds to K_i for the upstream rotor is 34.25°, which is between our measured values of β measured on a disassembled meter (22° to 38°).

Rotor	K_i [m^{-3}]	Re (Transition)	$C_{D0}^{'}$ [m^{-3}] (Non-linear)	$C_{D1}^{'}$ [m^{-3}] (Linear)	$C_{D2}^{'}$ [m^{-3}] (Linear)	$C_{B0}^{'}$ [kg/s^2]	$C_{B1}^{'}$ [m]
Upstream	397610	4450	383430	39843	-124390	0.0152	0.725
Downstream	480000	2500	Equation 20	119860	-273530	0.007	0.01

These results support the hypothesis that flow disturbances upstream from the second rotor require a more complicated model. However, as will be shown in the following section, correction terms are not necessary if the meter is used in the viscosity independent range of the calibration curve despite changes in the kinematic viscosity of the fluid being metered.
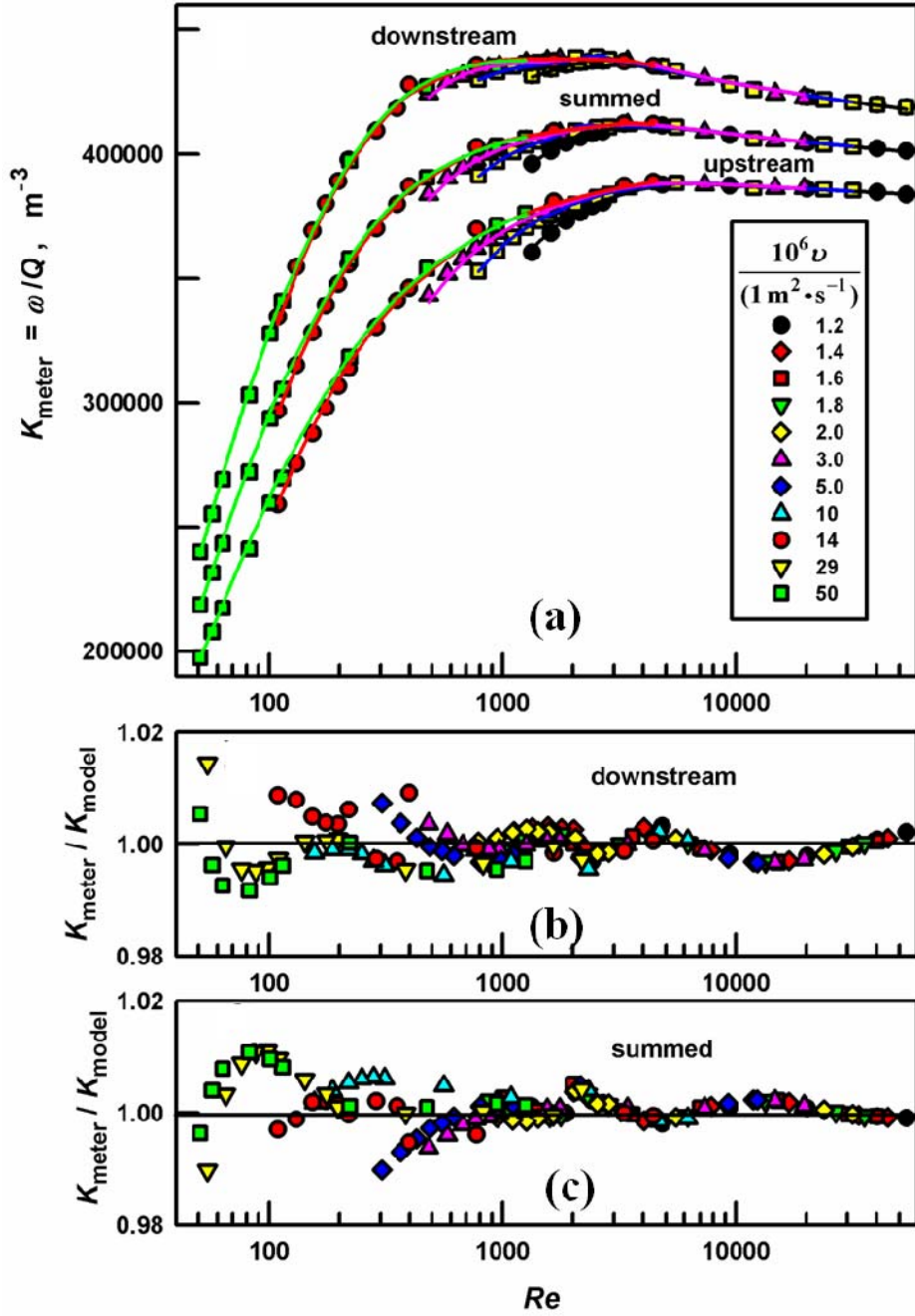
Figure 8: (a) Calibration curves for the upstream, downstream and summed rotors of the 2.5 cm diameter meter in this study. Some tested kinematic viscosities are omitted for clarity in (a) but are shown in (b) and (c). The summed rotor curve is plotted using the average meter factor ($K_{sum}/2$) for demonstration purposes. The lines are a fit to the experimental data (symbols) using the Lee model. (b) and (c) Ratio of computed to experimental values of K for the downstream and summed rotors respectively. The data for the upstream rotor is a subset of Figure 1 (not as low in flow) due to experimental limitations and to present comparable data sets for upstream, downstream, and summed rotors.

4.3 Sensitivity to Kinematic Viscosity in the Bearing Dependent Range

In the bearing dependent range of a turbine meter, using a single K vs. Re (or Strouhal vs. Roshko) curve can lead to large flow measurement errors in applications with variable kinematic viscosity due to the fanning phenomenon. In most of these situations, it will be necessary to use an approach that accounts for the bearing drag terms in the extended Lee model to obtain acceptable uncertainty. Errors can be introduced by 1) calibrating the meter in one viscosity liquid then using it in another, 2) using the meter in multiple liquids with different viscosities, or 3) using it in a single liquid at different temperatures (since $\nu = f[T]$).

To illustrate case 1, when we compared calibration curves of the 2.5 cm diameter meter from Stoddard solvent and a PG+W mixture of approximately equal kinematic viscosity, we found RMS differences of 0.46 % and the individual points differed by 0.29 % to 0.61 % in the bearing dependent range even though the kinematic viscosity of the PG+W mixture and Stoddard solvent in these experiments differed by only 0.018×10^{-6} m^2/s (1.5 %). This is due to the strong sensitivity of the meter factor on kinematic viscosity at low ν values in the bearing dependent range.

To demonstrate case 2, we examine the flow errors that would result by using a single K vs. Re (or St vs. Ro) curve for the 2.5 cm turbine data in Figure 1 for kinematic viscosities ranging from 50×10^{-6} m^2/s and 1.2×10^{-6} m^2/s. If one used a single K vs. Re curve that fell half way between the two viscosity extremes, the largest deviation from that curve is 16.7 % at the lowest Re value they share (≈ 539). Therefore, if the 1.2×10^{-6} m^2/s ν mixture was being metered, an overestimation in the K factor (and hence volumetric flow) of up to 16.7 % would occur. As shown in Figure 1(b), the largest error in the K factor using the Lee model in this range is 3.6 %. Therefore, the model gives the advantage that if the meter must be used in the bearing dependent range, the uncertainty in the K factor will be decreased by as much as 13.1 % for the range of viscosities tested here.

We can examine case 3 with another example. If the 2.5 cm diameter turbine meter studied here is calibrated in Stoddard solvent at 20 °C and later used to measure flow in the same fluid at a different temperature, temperature effects on the kinematic viscosity will change the K factor in the bearing dependent range. Figure 9 illustrates the deviation of the K factor at various temperatures from the K factor measured at 20 °C for Stoddard solvent as predicted by the fitted model for the 2.5 cm turbine meter. At the lowest flows that still rotate the rotor, a 10 °C temperature increase causes a 0.95 % change in the meter factor due to ν effects. This effect is nearly doubled for PG+W since its $\partial \nu / \partial T$ is approximately twice as large as Stoddard solvent's. We state this about PG+W not because we want to discourage replacement of Stoddard solvent, but to demonstrate

that the kinematic viscosity temperature dependence of the fluid being metered can greatly influence the uncertainty of flow measurement in this range.
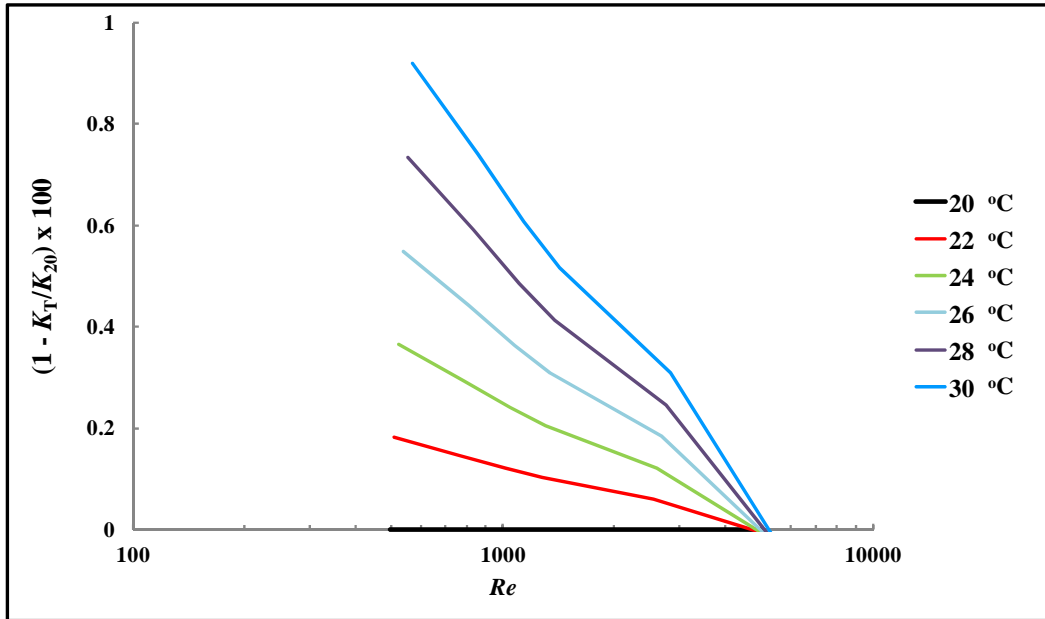

Figure 9: The K factor in the bearing dependent range is highly temperature dependent. Shown are deviations from the K factor in Stoddard solvent at 20 °C.

4.4. PG+W Mixtures Can Replace Hazardous Fluids

Next we consider more carefully whether PG+W mixtures can be used as surrogate fluids for Stoddard solvent, jet fuel, or hydraulic oils. As shown in Figures 1 and 8, at *Re* values larger than where the fanning occurs, the standard dimensionless quantities (see Appendix B) used for turbine meter calibrations collapse data for a wide range of fluid kinematic viscosities and more complex corrections based on the extended Lee model are not necessary. For the 2.5 cm diameter meter we tested and modeled, the RMS deviation of residuals of *K* versus *Re* plots using Stoddard solvent and PG+W mixtures is 0.056 % in the viscosity independent range and no individual point was more than 0.08 % different from the average *K* factor curve fit to the Stoddard solvent data, even though the kinematic viscosity of PG+W mixtures was varied from 1.2×10^{-6} m^2/s to 13.7×10^{-6} m^2/s (Figure 10). This is well explained by the extended Lee model: the dominant retarding torque in this range is the fluid drag term which is dependent on *Re* and hence the curves collapse despite the kinematic viscosity changes. In the bearing dependent range, the same calibration curve would result for two fluids with the same kinematic viscosity, but this is normally impractical to achieve and there is no strong advantage to using one liquid over another.

24

Unlike the prior calibration data presented, the sum of the two rotor frequencies of the dual rotor turbine is used here, a common practice for dual rotor turbine meter users. Our ability to obtain overlapping data for different fluids is constrained at the higher Re values by the upper flow limit of the 20 liter hydrocarbon liquid flow standard, especially for the higher viscosity fluids: if the fluid v is doubled, the tested flow must be doubled to obtain the same Re.

To compare results, a curve was fitted to the Stoddard solvent calibration data and the difference between the best fit and the calibration results for the various PG+W calibration points were calculated. These residuals are plotted in Figure 10(b) for the 2.5 cm diameter meter for Re values in the viscosity independent range of the turbine meter. The PG+W and Stoddard solvent calibrations agree within 0.08 %, within our expectations of 0.2 % based on property uncertainties and long term reproducibility of the flow meter. There is a systematic pattern to the residuals that we suspect is due to meter drift over the long delay (3 years) between measurements in the two fluid types. In another experiment, a 1.25 cm diameter, dual rotor, turbine meter was used to compare calibration curves generated using Stoddard solvent and a 1.2×10^{-6} m^2/s v PG+W mixture. For this meter we found that in the viscosity independent range, the difference between meter factors for the two fluids was within 0.02 %.

Based on these results, we conclude that if a turbine flow meter is used in its viscosity independent range, the difference between using PG+W mixtures and Stoddard solvent is negligible. As explained in section 4.3, turbine meters should not be used in the bearing dependent range unless the user accepts the errors of the calibration curve fanning caused by kinematic viscosity variations. Alternatively, a more complex calibration approach than K vs. Re (or Strouhal vs. Roshko) based on the fitted Lee model (Equation 18 or 21) could be used.
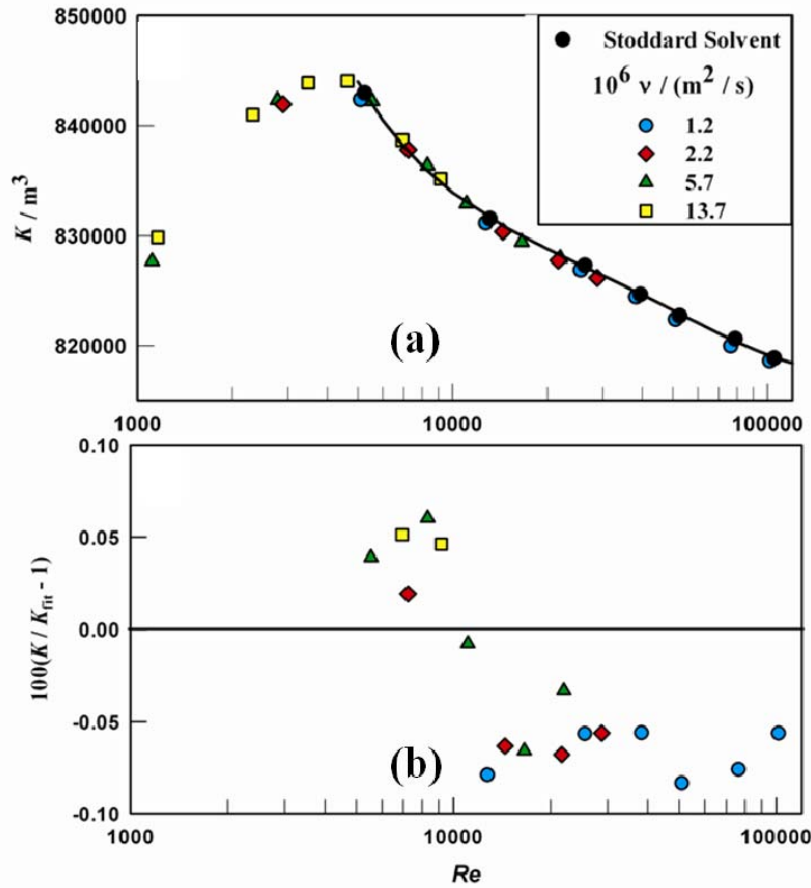
Figure 10: (a) Calibration curve showing the agreement between Stoddard solvent and PG+W mixtures. The solid line is a fit to the Stoddard solvent data. (b) The percent residuals between the Stoddard solvent data (0 % line) and four PG+W mixture data sets.

5. Conclusions

The influence of kinematic viscosity on turbine meter calibration curves has been of interest for more than 50 years [4, 6 - 11]. To date, there are no models that combine experimental data with the physics of the interactions between the fluid, rotor blades and the bearings to accurately explain why kinematic viscosity changes cause fanning of calibration curves at low *Re* numbers.

Equation 18 represents a physical model, termed the extended Lee model, of a turbine meter that incorporates 1) fluid drag on the rotor, 2) bearing static drag and 3) bearing viscous drag. The model accounts for the calibration curves generated from a 2.5 cm turbine meter using fluids of various kinematic viscosities and it correlates the volumetric flow within 0.2 % for *Re* > 3500. At *Re* < 3500, the fitted model matches the experimental data within 3.6 % despite corrections as large as 61 % of the ideal *K* factor. This gives us

confidence that the model captures the major physical phenomena and can be used to understand the complex behavior of turbine meter calibration curves.

PG+W is a suitable substitute for Stoddard solvent and other hazardous calibration fluids for calibrating turbine flow meters. This finding will enable laboratories that calibrate turbine meters for hydrocarbon liquid applications to stop using hazardous fluids in their meter calibration services. However, the model demonstrates that the presently used K vs. Re (or Strouhal vs. Roshko) methods for turbine calibrations cannot correct for two bearing drag effects that cause fanning at low flows. Also, we note that matching calibration and application kinematic viscosities will not correct the effects from varying kinematic viscosity caused by temperature changes during meter usage. For the example in Section 4.3 and illustrated in Figure 9, a 10 °C temperature change in Stoddard solvent will introduce a 0.95 % flow error if no corrections in bearing drag are used. Hence it is important to identify where the calibration curve fanning begins and to only use turbine meters above a meter specific Re value for low uncertainty applications. Otherwise, it is necessary to determine the values of the fluid and bearing drag terms' coefficients and use a more sophisticated flow calculation approach than the commonly used K vs. Re (or Strouhal vs. Roshko) methods.

Evaluation of turbine meters of different designs and sizes is needed to learn more about how results for the turbine meter studied here can be generalized. We expect that meters of different sizes with the same type of ball bearings will have similar characteristics in their calibration curves as the meter we studied because the size of the rotor and the bearings will vary in proportion to the designed maximum of momentum of the incoming fluid. Therefore, the model will be applicable to all meter sizes; however, this needs further investigation. Furthermore there is room for improvement of the model evidenced by patterns in the fit residuals, Figure 1(b). We hypothesize that the function of Re for the skin fluid drag term could be improved. For metering fluids in the viscosity independent range, the model is not needed to get a low uncertainty measurement. The model correlates the K factor within 0.2 % in this range for all the kinematic viscosities solutions tested, however, all the data points are within 0.062 % of a fitted line to all the measurements in this range. Therefore, the use of the model in this range is not advantageous. The extended Lee model does however greatly improve the uncertainty in measuring low flows that are in the bearing dependent range of the meter. For the model to be offered with a calibration service, a meter specific function fitted to the residuals of the model in the bearing dependent range can be determined to further improve uncertainties leading to replacement of the presently used calibration schemes and allow measurements better than 0.5 % over a wide range of flows and kinematic viscosities.

Appendices

Appendix A: Derivation of Bearing Drag Terms:

Bearing torques can be written as:

$$T_B = C_{B0} + C_{B1}\rho v \omega + C_{B2}\omega^2.$$
(A1)

Coulomb or static drag can be found described in basic textbooks [15]. This torque can be written as:

$$C_{B0} = \frac{kq1q2}{r}$$
(A2)

Where k is a proportionality constant, $q1$ and $q2$ are the net charges on the surfaces of the rotational axis and the ball bearings respectively and r is the distance between the rotational axis and the ball bearings.

Viscous drag on bearing load has been described in the literature [16, 17] such that:

$$C_{B1} = \frac{4\pi R_1^2 R_2^2}{R_2^2 - R_1^2} L,$$
(A3)

where R_1 and R_2 are the inner and outer ball bearing race radii respectively. L is the length of the bearing along the axis of rotation.

The third term considered is that due to axial thrust and dynamic imbalance. Mathematical expressions for both can be added together as they are both a function of ω^2. The axial thrust is a force that is a function of the rate of change of mass with respect to time and the speed of the fluid moving through the rotor blades. This can be written as a torque by recognizing that the angle between the force vector and the "lever arm" vector is 90° and that R_2 as defined above is the magnitude of the lever arm vector. Therefore the torque due to axial thrust can be expressed as:

$$T_{AT} = \omega^2 \rho R_2 \pi \bar{r}^{-4}.$$
(A4)

The torque on the rotor system due to dynamic imbalance has been derived in detail by Yuru et. al. [18]:

28

$$T_{DI} = \frac{m_B R_2^2 \omega^2}{4\pi}.$$ (A5)

Adding the torque due to axial thrust (Equation A4) with that due to dynamic imbalance (Equation A5), one obtains:

$$T_{B2} = \left(R_2 \pi \bar{r}^{-4} \rho + \frac{m_B R_2^2}{4\pi} \right) \omega^2.$$ (A6)

Since the density for the PG+W mixtures is approximately the same for all viscosities covered [12] and because this term should be negligible in a meter with a well designed rotor system, the term in parenthesis can be considered a constant such that:

$$C_{B2} = R_2 \pi \bar{r}^{-4} \rho + \frac{m_B R_2^2}{4\pi}.$$ (A7)

Inserting Equations A2, A3 and A7 into Equation A1 and dividing by $\bar{r}^2 \rho Q^2$ gives the total torque exerted on the rotor system due to the bearings:

$$\frac{T_B}{\bar{r}^2 \rho Q^2} = \frac{C_{B0}}{\bar{r}^2 \rho Q^2} + \frac{C_{B1} \nu \omega}{\bar{r}^2 Q^2} + \frac{C_{B2} \omega^2}{\bar{r}^2 \rho Q^2}.$$ (A8)

$\bar{r}^2$ can be included in the constants such that $C_{B0}' = C_{B0}/\bar{r}^2$, $C_{B1}' = C_{B1}/\bar{r}^2$ and $C_{B2}' = C_{B2}/\bar{r}^2$. Therefore:

$$\frac{T_B}{\bar{r}^2 \rho Q^2} = \frac{C_{B0}'}{\rho Q^2} + \frac{C_{B1}' \nu \omega}{Q^2} + \frac{C_{B2}' \omega^2}{\rho Q^2},$$ (A9)
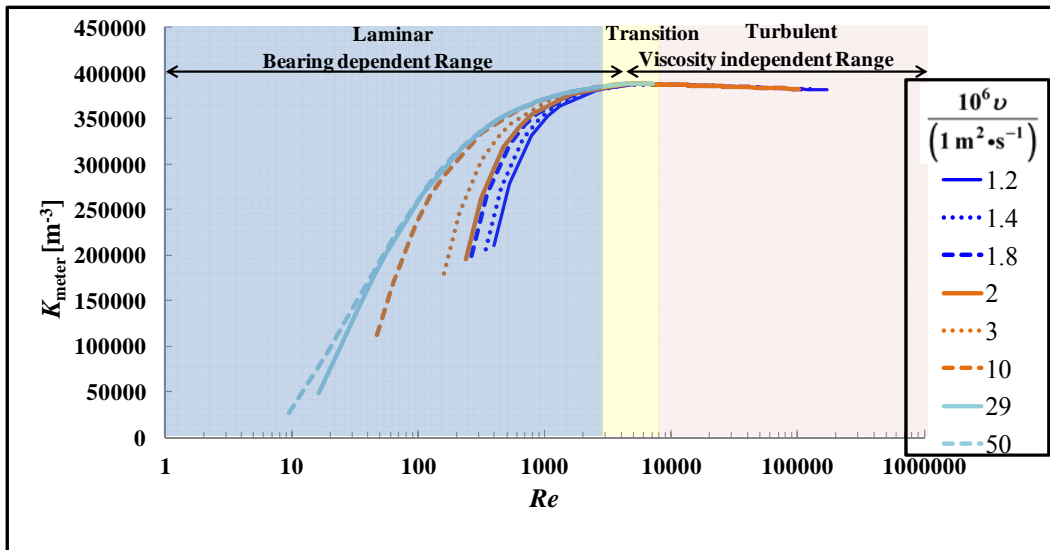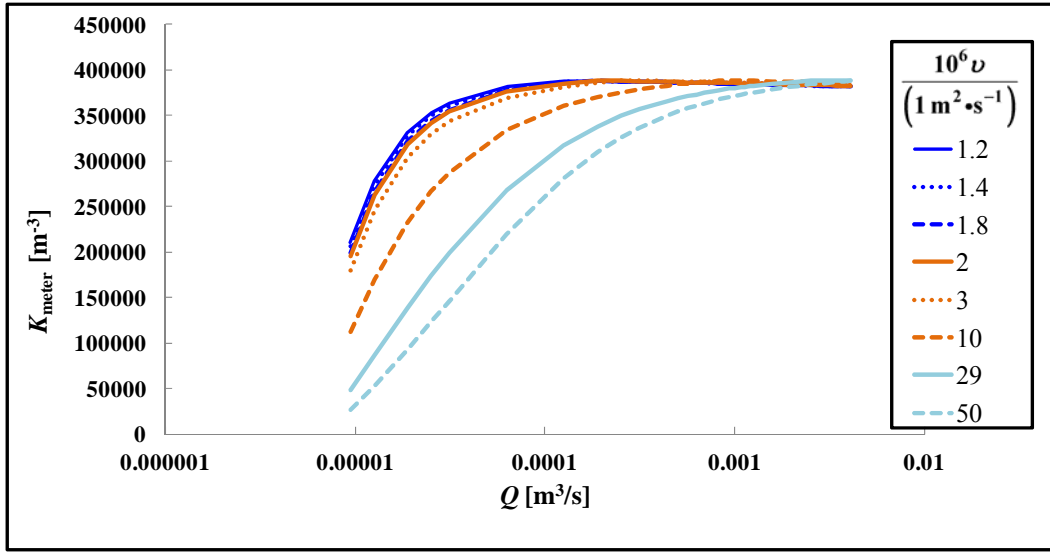
which is Equation 17 in the text.

For practical turbine meter calibrations, a K factor based on a frequency output by the passage of each rotor blade is used (K_f) and since, $f = \omega N/(2\pi)$ (where N is the number of blades on the rotor) these two versions of the K factor are related by:

$$K_f = \frac{f}{Q} = \frac{N\omega}{2\pi Q} = \frac{N}{2\pi}K. \tag{B1}$$

Applying dimensional analysis to fluid dynamics problems to identify dynamic similitude between different test cases leads to the dimensionless quantities: Strouhal (St) and Re or Roshko (Ro) numbers. This dimensionless parameterization for turbine meter calibration curves leads to the collapsing of the curves in the viscosity independent range despite differences in the fluid properties. The difference in the curves in Figure B1 demonstrates the great advantage this provides for calibration curves. Figure B1(a) demonstrates the ranges of Re that define the laminar, transition, turbulent, bearing dependent and viscosity independent ranges of the curves. The Re value at which these regimes or ranges occur are meter specific. It is common to hear the term "universal viscosity curve (UVC)" when referring to a turbine meter's calibration curve. However, we have chosen not to use this term as it does not hold true for all ranges of the curve and thus we use the term "viscosity independent range" that covers the part of the curve that is viscosity independent and the term "bearing dependent range" to define the portion of the curve that is not viscosity independent due to drags acting on the rotor that are highly influenced by the kinematic viscosity.

(a)

(b)

Figure B1: Comparison of a turbine meter's calibration curve plotted using Re (a) and volumetric flow (b).

The figures presented in this paper use K and Re since Re is the appropriate quantity for fluid drag coefficients and the prior literature on turbine meter physical models use the meter factor. However, it is also common to use the dimensionless numbers St and Ro to present turbine meter calibration data and they would work as well. Here we give the relationships between these quantities.

The Strouhal number is a dimensionless form of the K factor:

$$St = \frac{K_f \pi d^3}{4},$$ (B2)

where d is the diameter of the meter casing. Ro is the product of St and Re:

$$Ro = \frac{f d^2}{\nu}$$ (B3)

In cases where a wide range of temperatures is expected, thermal expansion effects on the diameter can be applied:

$$d(T) = d_0 \left[1 + \alpha (T - T_0) \right]$$ (B4)

where d_0 is the diameter at a reference temperature T_0 and α is the thermal expansion coefficient of the meter.

Replacing *Re* on the x-axis with *Ro* does not alter the shape of the curve since it is proportional to *f/v*, *Re* is proportional to *Q/v*, and *f* is proportional to *Q* as mentioned in the text until the flow decreases to almost the point of not turning the rotor. In practical applications of turbine meter calibration curves, *Ro* is preferable to *Re* since *Ro* does not include the flow while using *Re* requires an iterative process to obtain a low uncertainty meter factor. By using *Ro*, when a customer is presented with a meter calibration curve, the frequency readout and the kinematic viscosity is all that is needed to determine the flow from the *St* (or *K*) value.

References

[1] Measurement of Liquid Hydrocarbon by Turbine Meter Systems. American Petroleum Industry Standard 2534, 1970.

[2] Latsko J, Winchester J. Accounting for the Impact of Thermal Instability in the Liquid Comprising the Connecting Volume of a Piston Displacement Type Volumetric Flow Rate Standard. NCSLI Annual Conference Proceedings 2010.

[3] Stoddard Solvent Public Health Statement. Agency for Toxic Substances and Disease Registry, Center for Disease Control. http://www.atsdr.cdc.gov/ToxProfiles/tp79-c1.pdf.

[4] Ball J. Turbine Flow Meter Calibration Using Nonpolluting Fluid Mixtures to Simulate Fuels and Lubricants. Cal Lab the International Journal of Metrology 2011; 18: 32-36.

[5] Johnson AN, Crowley CJ, Yeh TT. Uncertainty Analysis of NIST's 20 Liter Hydrocarbon Liquid Flow Standard. Journal of the Metrology Society of India 2011; 26: 187-202.

[6] Lee WFZ, Evans, HJ. Density Effect and Reynolds Number Effect on Gas Turbine Flowmeters. Journal of Basic Engineering 1965; 1043-57.

[7] Lee WFZ, Karlby H.   A Study of Viscosity Effect and Its Compensation on Turbine-Type Flowmeters. Journal of Basic Engineering, 1960; 717-27.

[8] Rubin M, Miller RW, Fox WG. Driving Torques in a Theoretical Model of a Turbine Meter. Journal of Basic Engineering 1965; 413-20.

[9] Baker RC. Turbine flowmeters: II. Theoretical and Experimental Published Information. Flow Measurement and Instrumentation 1993, 4: 123-44.

[10] Tsukamoto, H and Hutton, SP. Theoretical Prediction of Meter Factor for a Helical Turbine Flowmeter, Conference on Fluid Control and Measurement, Tokyo, Japan, September 1985.

[11] Mattingly GE. Improved Meter Performance Charaterizations for Liquid and Gas Turbine Meters. Proceedings of the International Symposium on Fluid Flow Measurement 2009.

[12] Yang C, Ma P, Tang D, Jin F. Excess Molar Volume, Viscosity and Heat Capacity for the Mixture of 1,2-Propanediol-Water at Different Temperatures. Chinese J. Chem. Eng. 2003; 11: 175-80.

[13] Jimenez J, Martinez F. Study of Some Volumetric Properties of 1,2-Propanediol + Water Mixtures at Several Temperatures. Rev. Col. Cienc. Quim. Farm. 2005; 1: 46-57.

[14] Wadlow D. Turbine and Vane Flowmeters, In: J.G. Webster, editors. The Measurement, Instrumentation and Sensors Handbook, Boca Raton, FL: CRC Press; Dec. 1998, Chapter 28.4.

[15] Wolfson R , Pasachoff JM. Physics for Scientists and Engineers. 2nd ed. New York: Harper Collins College Publishers; 1995.

[16] Wang Z, Zhang T. Optimization of Geometric Parameters of the Rotor in the Turbine Flowmeter. Flomeko 15th Annual Conference Proceedings, 2010.

[17] Fuller, DD. Fluid Film Bearings, In Baumeister and Marks. Standard Handbook For Mechanical Engineers, New York: McGraw – Hill; 1967, p. 8-156 – 8-177.

[18] Yuru S, Mingzhi L, Hangxin W. Analysis of Static and Dynamic Imbalance in Rotor System. Proceedings of the First Asia International Symposium on Mechatronics, 2004.